# Numerical Simulation of External MHD Generator on Board Reentry Vehicle

Gang Chen, Huaping Zhen, Xiaoxuan Li, Wei Su, and Chao Dong
Beijing Institute of Space Long March Vehicle, Beijing, China
Email: chengang107@gmail.com, tracypp16@163.com

***Abstract*—A scenario of external magneto hydrodynamic (MHD) generator on board blunt-cone based re-entry vehicles was proposed, and numerical parametric studies by employing an MHD model based on the low magnetic Reynolds number approximation were performed. Following the numerical results, the physical features of the external MHD generator were drawn. One may conclude that the power output of the external MHD generator is capable of providing energy output up to 1.28MW under the typical reentry condition (flight height 46km, velocity7km/s). Under the MHD power extracting operation, the drag coefficient of the reentry vehicle is raised by 13. 7%, whereas the total wall heat flux varies mildly. However, the distribution of heat flux density in the MHD power extraction zone and downstream differs distinctly from that in the original N-S flow. The peak heat flux densities in the area occur at the tips of the electrodes.**

***Index Terms*—reentry vehicle, external MHD generator, magnetic Reynolds number, power extraction**

## I. Introduction

The utilization of plasmas for enhancing and controlling re-entry vehicle performances has been investigated in several papers [1]-[7]. There are two primary types of applications for this kind of hypersonic flow control concepts, namely, (1) the utilization of off-body plasmas for drag reduction and steering [1]-[4]; (2) the use of near surface plasmas combined with magnetic field for heat flux management [5-7]. For real sized vehicles, the energies required for these applications exceed the present capability of on-board auxiliary power units. Therefore, it is necessary for the re-entry vehicle to equip with an onboard power supply system.

In the high Mach number regime during a re-entry flight, say, for Ma$\geqslant$15 , there is sufficient heating of the gas surrounding the vehicle to sustain the MHD power extraction process using simply the equilibrium ionized alkali vapor seed material. Therefore, it is feasible to make use of an external MHD generator as the onboard power supply system, provided that a magnetic field system is appropriately arranged together with current collecting electrodes, the electric power can be extracted directly from the hypersonic gas passing over the vehicle.

Manuscript received July 1, 2015; revised October 14, 2015.

An external MHD generator based on a blunt-cone-shaped vehicle configuration was first conceptually considered by Bityurin, Bocharov, and Lineberry [8]. In several recent papers [9]-[12], computational fluid dynamics was employed to explore the power density level of external MHD generators during planetary re-entry. Results showed that megawatt power levels can be generated with a small amount of potassium seed (~1%) and modest values of magnetic field (0.1~0.2Tesla) [9]. However, a systematic deduction for generator design factors and their influences on the generated power have not been founded at the present stage. In addition, in above mentioned papers, the electric field in the region between electrodes was either assumed uniform, or was evaluated by solving solely the Poisson equation. The decoupling from flow equations means that the influences of the electromagnetic field upon the flow field were neglected.

In the present paper, efforts will be focused on the coupled simulation of an external magneto hydrodynamic (MHD) generator on board blunt-cone based re-entry vehicles. Following the numerical results, the physical features of the external MHD generator were drawn.

## II. Scenario of External MHD Generator

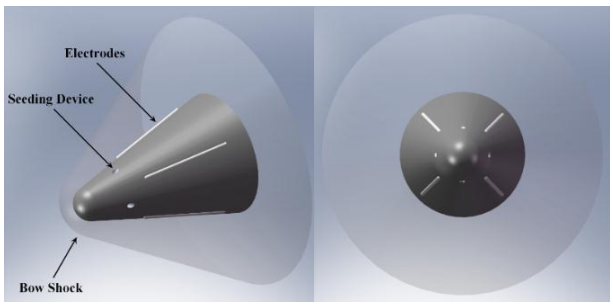


Figure 1. The scenario of external MHD generator

Consider a blunt-cone based re-entry vehicle as shown in Fig. 1: nose radius $R_n = 0.12m$ , half cone angle $\theta = 12^\circ$ , and vehicle length $L = 1.62m$ . Refer to the external generator scheme proposed by Ref [13-15], four electrodes are arranged evenly along the circumferential direction. The width of the electrodes $W_E = 0.2094R$ (Where R is the local section radius), the electrodes length $L = 0.7m$ .



doi: 10.18178/joace.4.4.273-278

In a probable "real" external MHD generator, the magnetic field is likely provided by electromagnetic coils beneath the vehicle wall. In this paper, the coils were modeled by the combination of 4 infinite long straight current lines, which lie at 10cm beneath the electrodes with opposite current directions. The magnetic field vector distribution at the section x=0.2m is shown Fig. 2. The similarity of the magnetic field with the coils is obvious.

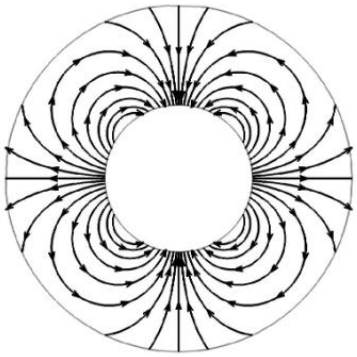

Figure 2. The magnetic field vectors distribution in the section at x=0.2

Upstream of the power extraction region, there are alkali vapor jet holes to strengthen the ionization of the gas flow. According to the conductivity distribution model in Ref [11, 13], a simplified Gauss distribution model was used in the simulation

$$\sigma(y)=\sigma_{y0}\exp\left[-a\left(y-y_0\right)^2\right] \tag{1}$$

In which y is the normal distance to the wall, $\sigma_{y0}$ is the conductivity value corresponding to the wall distance of $y_0$, Gauss distribution control parameter a

$$a=\lg\left(\sigma_{y0}/\varepsilon\right)/\delta^2 \tag{2}$$

In this paper, $y_0=0.03m$, $\sigma_{y0}=500S/m$, $\varepsilon=25S/m$, $\delta=0.05m$.

In this regime of hypersonic boundary layer flows(T≈ 3000~5000K seeded with 1% of alkali vapor), electron mobility $\mu_e\approx 2\sim 3T^{-1}$, ion mobility $\mu_i\ll 1$ [11]. According to this, Hall parameter and ion slip parameter can be calculated.

## III. Computational Model

### A. Governing Equations

The most general form describing the MHD flows consists of Navier-Stokes and Maxwell Equations. The Navier-Stokes equations including the electromagnetic effects as the forcing terms can be written as

$$\frac{\partial\rho}{\partial t}+\nabla\bullet(\rho\mathbf{U})=0$$

$$\begin{aligned}&\frac{\partial(\rho\mathbf{U})}{\partial t}+\nabla\bullet\left(\rho\mathbf{UU}+p\mathbf{I}-\frac{1}{\mathrm{Re}}\boldsymbol{\tau}\right)=Q(\mathbf{J}\times\mathbf{B})\\&\frac{\partial(\rho e)}{\partial t}+\nabla\bullet\left[(\rho e+p)\mathbf{U}\right]=\frac{1}{\mathrm{Re}}\nabla\bullet\left[\mathbf{U}\boldsymbol{\tau}+\frac{1}{(\gamma\text{-}1)\mathrm{PrM}_\infty^2\mathrm{Re}}\nabla T\right]+Q(\mathbf{E}\cdot\mathbf{J})\end{aligned} \tag{3}$$

where $\rho$, $\mu$, **U,** e, and $\boldsymbol{\tau}$ are, respectively, the density, viscosity, velocity vector, specific total energy, and the stress tensor of the fluid; **E** denotes the electric field, **J** the current density, and **B** is the magnetic field; and the magnetic interaction number is defined as Q=σ B L / ρ U, in which $\sigma_{ref}$ and $L_{ref}$ are the referential conductivity and length.

For low magnetic Reynolds number MHD flows, the induction magnetic field can be neglected. Then, Maxwell's equations given [13]

$$\begin{aligned}&\nabla\cdot\mathbf{J}=0\\&\mathbf{J}=\boldsymbol{\sigma}(\mathbf{E}+\mathbf{U}\times\mathbf{B})\\&\nabla\times\mathbf{E}=-\frac{\partial\mathbf{B}}{\partial t}=0\end{aligned} \tag{4}$$

By introducing an electric potential φ such that $\mathbf{E}=-\nabla\varphi$, the electric field can be governed by a Poisson equation

$$\nabla\cdot\mathbf{J}=\nabla\cdot\left[\boldsymbol{\sigma}(\mathbf{E}+\mathbf{U}\times\mathbf{B})\right]=\nabla\cdot\left[\boldsymbol{\sigma}(-\nabla\varphi+\mathbf{U}\times\mathbf{B})\right]=0 \tag{5}$$

where the conductivity **σ** is a tensor [14]. Thus, the flow and electromagnetic fields can be solved successively using Eq. (3) and (5).

### B. Numerical Method

A Navier-Stokes solver based on TVD scheme developed by this research group [15] is modified to incorporate MHD effects, corresponding to Eq. (3). The Poisson equation (5) is discretized using second-order central differencing scheme, with which a 19-point stencil is obtained, and solved by the successive over relaxation (SOR) method.

Several test cases were performed for validating the integrated solver developed for solving Eq. (3) and (5) simultaneously. The results are given as follows:

The first case is taken from Refs.14 and 16 to verify the Poisson solver. Consider a channel flow whose bounding walls are comprised of segmented electrodes separated by regions of insulating material. The electrodes are assumed to be 0.5 units long with equal spacing between successive elements as depicted in Fig.3. The distance between the walls is unity. A periodic array of electrodes is considered, and the potential gradient is chosen to be dφ/dx=0.4 along the axial direction. The velocity field is given to be u=u (y) and the conductivity is assumed to be uniform.

Fig. 4 depicts the potential contours and the current line distributions computed by the present work. The results are in good agreement with the results given in Ref. 14 and 16.

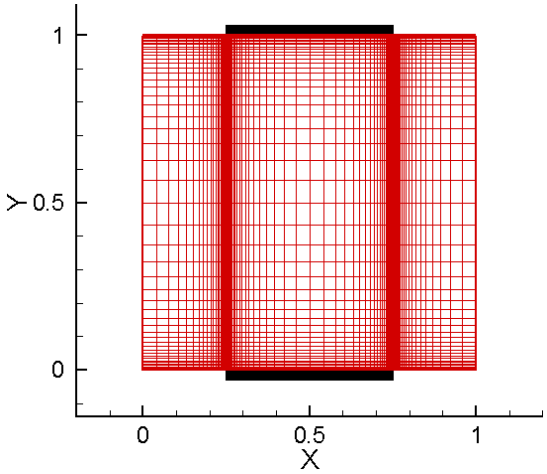


Figure 3. Grid for flow in channel with segmented electrodes.

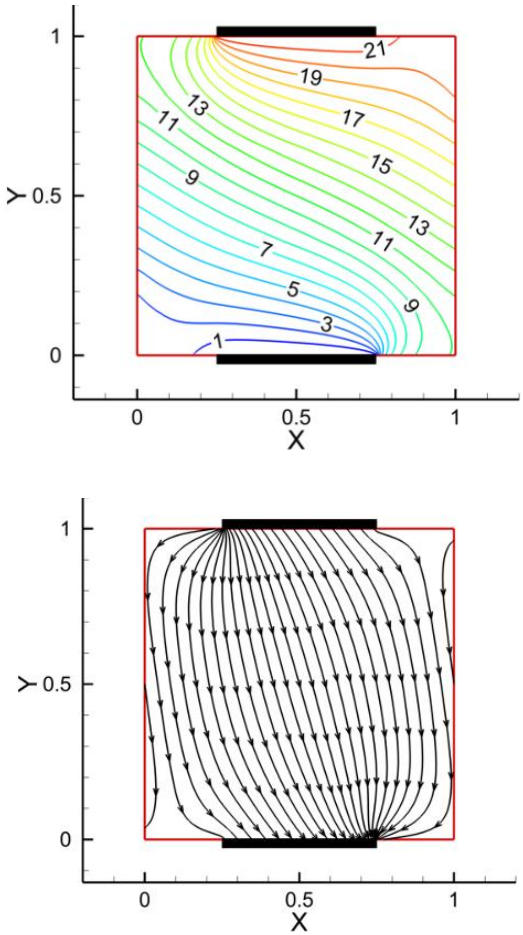


Figure 4. Potential contours (upper) and current density stream ntraces (lower) at Hall parameter=5, Ion slip parameter=5.

The second case is a Hartmann flow problem as depicted in Fig. 5 (cf., Ref. 13 for details). Numerical simulations were conducted on two different meshes, where the coarse grid consists of $10\times50\times3$ points, and the fine mesh consists of $30\times80\times3$ points.

The comparison between the numerical results computed by the present work and analytic solutions are illustrated in Fig. 6. It is seen that the numerical solutions with different values of Hartmann numbers are practically overlapping with the respective analytic solutions, which demonstrates that the present solver possesses excellent accuracy and grid independency.

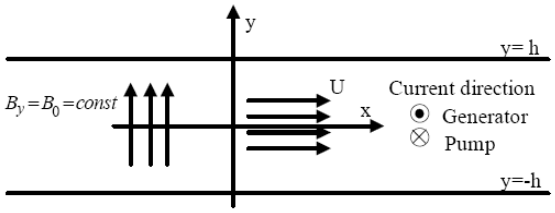


Figure 5. Sketch of hartmann flow.

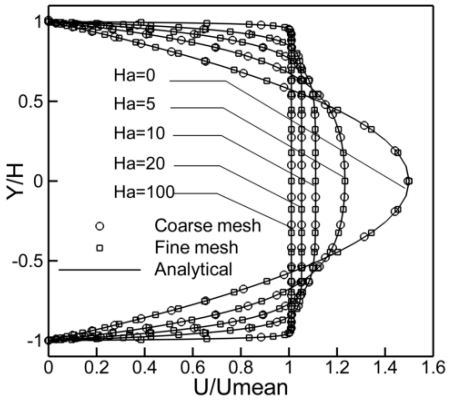


Figure 6. Velocity profiles of Hartmann flow.

## IV. Results and Discussion

### A. Case Setup

Simulation parameter: h=46km, Ma=21.37, $T_{wall}$ =1000K, referential magnetic field strength $B_{ref}$=0.2T; Magnetic interaction number (per unit length) $N_1$=1.67, electric potential on the anode and cathode are respectively 100V and 0V. Fig. 7 shows the mesh and electrodes.

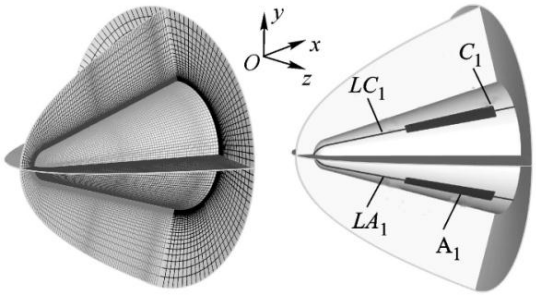


Figure 7. Grid and electrodes

### B. Electrical Characteristics of External MHD Generator

The computed potential contours and current vector field are given, respectively, in Fig. 8 and Fig. 9. The two pictures depict the fundamental physical features: driven by $\mathbf{U}\times\mathbf{B}$, motive electric currents come out from the cathodes and flow toward the anode. Between the electrodes, the electric currents concentrate in the ring region corresponding to the high conductivity. The distribution both of φ and **J** have ax symmetric

characteristics, which means that the Lorentz force and Joule heating effect on the flow field is also ax symmetric.

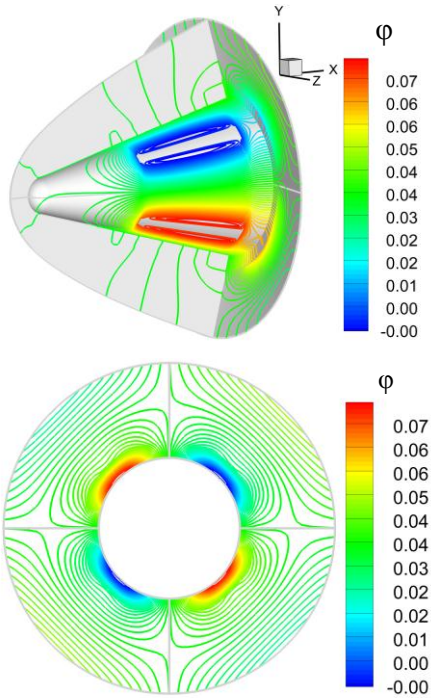


Figure 8. Electric potential contours, total distribution (upper) and details at the section with x=1.0 (lower)

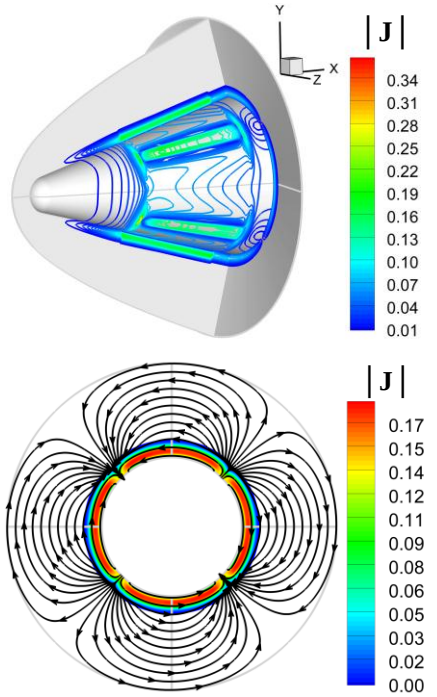


Figure 9. Scalar current densities, total distribution (upper) and details at the section with x=1.0 (lower)

Fig. 10 shows the Jz variation with wall distance in the upper half of the x-y symmetric plane. Note J denotes the grid index along the wall normal direction. There exist currents flowing from the anode to the cathode in the rear region of the electrodes, which are called leaking currents. These leaking currents and the electric motive currents between the electrodes form the electric current vortices, which are shown in Fig. 11. This could be minimized by lengthen the magnetic field region.

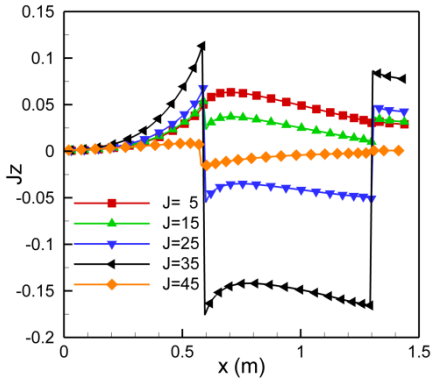


Figure 10. Jz variation with wall distance in the upper half of the x-y symmetric plane

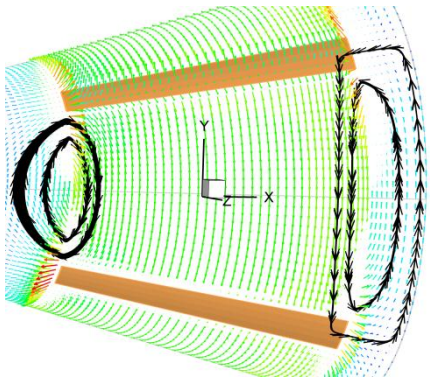


Figure 11. The electric current vortices

In the near wall region between the electrodes, there are also leaking electric currents caused low velocities. Fig. 12 gives the electric current vectors and stream lines at the section with x=1.0m. One can find the static electric current in the near wall region.

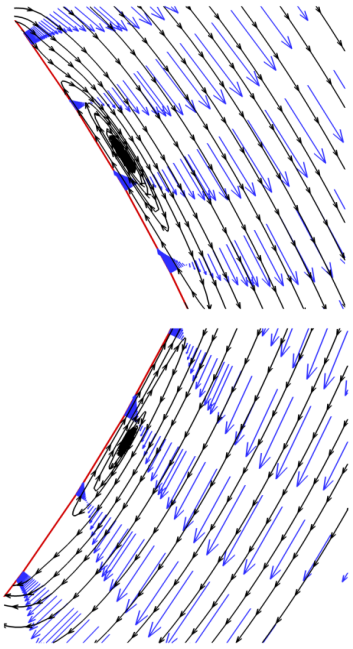

Figure 12. Section at x=1.0m, upper: Cathode; lower: Anode

According to Ohm's law, the energy transformation relation in a external MHD generator can be written as follows:

$$\begin{aligned}\mathbf{E}\bullet\mathbf{J} &= \mathbf{J}\bullet\left[\mathbf{J}/\sigma-(\mathbf{U}\times\mathbf{B})+\beta(\mathbf{J}\times\mathbf{B})-\alpha(\mathbf{J}\times\mathbf{B}\times\mathbf{B})\right] \\ &= J^2/\sigma+(\mathbf{J}\times\mathbf{B})\bullet\mathbf{U}-\alpha\left[(\mathbf{J}\bullet\mathbf{B})^2-J^2B^2\right]\end{aligned} \quad (6)$$

In which (J×B)•U is the power of Lorentz Force, E•J is the electric power, $J^2/\sigma-\alpha[(J\bullet B)^2-J^2B^2]$ is the Joule heating power, which is always positive. In a generator device, (J×B)•U<0, E•J<0. Therefore, the Lorentz force extracts power from the flow field and transforms it to electric power. During this process, Joule heating is always an inevitable loss. The extracted power $P_{Extract}=-\iiint_V \mathbf{E}\bullet\mathbf{J}\,dv$, the Joule heating power $P_{Joule}=\iiint_V J^2/\sigma-\alpha\left[(\mathbf{J}\bullet\mathbf{B})^2-J^2B^2\right]dv$, the total power contributed by Lorentz force $P_{EM}=\iiint_V(\mathbf{J}\times\mathbf{B})\bullet\mathbf{U}\,dv$, the electric efficiency $\eta=-P_{Extract}/P_{EM}$.

In the simulation case of this paper, the extracted power $P_{Extract}=1.28MW$, the electric efficiency $\eta=29.4\%$. The result reveals that the proposed external MHD generator could extract Megawatts power from the hypersonic surrounding flows.

### *C. Influence of Power Extraction on Aerodynamic Force and Heating*

Table I shows the comparison of aerodynamic coefficients with and without power extraction. Due to the power extraction operation, the wave drag rises by 7.3%, the friction drag decreases by 12.7%. However, the effect of power should also include the electromagnetic counter force mounted on the onboard coils, which could be calculated as follows,

$$\mathbf{F}_{EM}=-\iiint_V(\mathbf{J}\times\mathbf{B})dv \quad (7)$$

The electromagnetic force coefficient in this case equals 0.0221. Considering this, the total drag of the vehicle rises by 13.7% due to the power extraction.

TABLE I. COMPARISON OF AERODYNAMIC COEFFICIENTS

| aerodynamic coefficients | N-S | MHD | Discrepancy (%) |
|---|---|---|---|
| Wave Drag | 0.150 | 0.161 | 7.3 |
| Friction Drag | 0.00864 | 0.00754 | -12.7 |
| Electromagnetic force | | 0.0221 | |

As refer to the wall heat flux, there are two key factors: (1) the local inviscid flow velocity and temperature ;(2) the mechanism of power transformations in the viscous boundary layer.

Starting from this, MHD power extraction has two opposite effect on wall heat flux:(1) the deceleration effect of Lorentz force on the flow could mitigate the velocity gradient in the boundary layer flow, an then weaken the dissipation mechanism in the near wall region; (2) Joule heating increases the inviscid flow temperature and introduce another new dissipation mechanism.

The heat flux density distribution of the half vehicle is shown in Fig. 13. Compared to the flow field without MHD power extraction, the heat flux density rises by 30% near the tip of the electrodes due to the Joule heating. In some local region between the electrodes, aerodynamic heating are mitigated by the MHD power extraction.

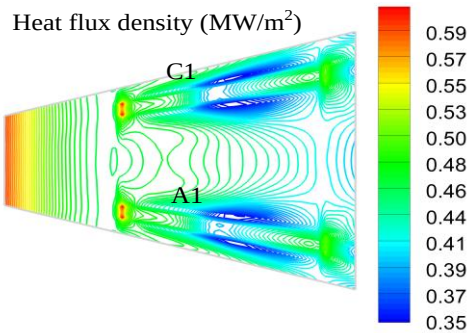


Figure 13. Wall heat flux density distribution(z≥0)

## V. CONCLUSION

A scenario of external Magneto Hydrodynamic (MHD) generator on board blunt-cone based re-entry vehicles was proposed in this paper, and numerical parametric studies by employing an MHD model based on the low magnetic Reynolds number approximation were performed. Following the numerical results, the physical features of the external MHD generator were drawn. The simulation results showed that:

(1) The power output of the external MHD generator is capable of providing energy output up to 1.28MW under the typical reentry condition (flight height 46km, velocity7km/s).

(2) With the MHD power extracting operation, the drag coefficient of the reentry vehicle is raised by 13. 7%, whereas the total wall heat flux varies mildly. However, the distribution of heat flux density in the MHD power extraction zone and downstream differs distinctly from that in the original N-S flow. The peak heat flux densities in the area occur at the tips of the electrodes.

## REFERENCES

[1] D. Knight, V. Kuchinskiy, V. Kuranov, et al. "Survey of aerodynamic flow control at high speed by energy deposition," AIAA-2003-0525, 2003.

[2] R. B. Miles, S. O. Macheret, M. N. Shneider, et al. "Plasma-enhanced hypersonic performance enabled by MHD power extraction,"AIAA-2005-561, 2005

[3] I. G. Girgis, M. N. Schneider, S. O. Macheret, et al. "Steering moments creation in supersonic flow by off-axis plasma heat addition," *Journal of Spacecraft and Rockets*, 2006, vol. 43, no. 3, pp. 607-613

[4] N. J. Bisek, I. D. Boyd, J. Poggie, "Numerical study of energy deposition requirements for aerodynamic control of hypersonic vehicles," AIAA-2008-1109, 2008

[5] D. Knight, "A selected survey of magnetogasdynamic local flow control at high speeds," AIAA-2004-1191, 2004

[6] V. A. Bityuri, A. N. Bocharov, D. S. Baranov, et al. "Study of MHD flow control and on-board electrical power generation," AIAA-2006-1008, 2006
[7] V. A. Bityurin, A. N. Bocharov, "MHD flow control in hypersonic flight," AIAA-2005-3225, 2005
[8] G. W. Garrison, "The electrical conductivity of a seeded nitrogen plasma," *AIAA Journal 1968*, vol. 6, no. 7, pp. 1264-1270
[9] F. K. Lu, H. C. Liu, and D. R. Wilson, "Electrical conductivity channel for a shock tube," *Measurement Science Technology*, vol. 16, no. 9, pp. 1730-1740, 2005.
[10] V. A. Bityurin, V. A. Zeigarnik, and A. L. Kuranov, "On a perspective of MHD technology in aerospace applications," AIAA-96-2355, 1996
[11] S. O. Macheret, M. N. Shneider, and G. V. Candler, "Modeling of MHD power generation on board reentry vehicles," AIAA-2004-1024, 2004
[12] C. A. Steeves, H. N. G. Wadley, R. B. Miles, et al. "A magneto-hydrodynamic power panel for space re-entry vehicles," *J Appl Mech*, vol. 74, no. 26, pp. 57-64, 2007.
[13] C. A. Steeves, M. N. Shneider, S. O. Macheret, et al. "Electrode design for magneto hydrodynamic power panels on reentering space vehicles," AIAA-2005-1340, 2005
[14] T. Wan, R. Suzuki, G. V. Candler, "Three dimensional simulation of electric field andMHD power generation during re-entry," AIAA-2005-5045, 2005
[15] G. Chen, C. H. Lee, J. B. Zhang, et al. "Modeling and parametric studies of external MHD generators," AIAA-2009-1233, 2009
[16] G. W. Sutton and A. Sherman, *Engineering Magneto Hydrodynamics*, New York: McGraw Hill, 1965, pp. 295-308
[17] D. V. Gaitonde, "A high-order implicit procedure for the 3-D electric field in complex magnetogasdynamic simulations," *Comp Fluids*, vol. 33, no. 3, pp. 345-374, 2004.
[18] B. Zheng and C. H. Lee, "The effects of limiters on high resolution computations of hypersonic flows over bodies with complex shape," *Comm Nonlinear SciNumer Simul*, vol. 3, no. 2, pp. 82-87, 1998.

 